



**HAL**  
open science

## Synchronization in spiking neural networks with short and long connections and time delays

Lionel Kusch, Martin Breyton, Damien Depannemaecker, Spase Petkoski,  
Viktor K Jirsa

► **To cite this version:**

Lionel Kusch, Martin Breyton, Damien Depannemaecker, Spase Petkoski, Viktor K Jirsa. Synchronization in spiking neural networks with short and long connections and time delays. *Chaos: An Interdisciplinary Journal of Nonlinear Science*, 2025, 35, 10.1063/5.0158186 . hal-04947885

**HAL Id: hal-04947885**

**<https://hal.science/hal-04947885v1>**

Submitted on 14 Feb 2025

**HAL** is a multi-disciplinary open access archive for the deposit and dissemination of scientific research documents, whether they are published or not. The documents may come from teaching and research institutions in France or abroad, or from public or private research centers.

L'archive ouverte pluridisciplinaire **HAL**, est destinée au dépôt et à la diffusion de documents scientifiques de niveau recherche, publiés ou non, émanant des établissements d'enseignement et de recherche français ou étrangers, des laboratoires publics ou privés.









Distributed under a Creative Commons Attribution - NonCommercial - NoDerivatives 4.0  
International License

RESEARCH ARTICLE | JANUARY 30 2025

## Synchronization in spiking neural networks with short and long connections and time delays

Special Collection: [Disruption of Networks and System Dynamics](#)

Lionel Kusch ; Martin Breyton ; Damien Depannemaecker ; Spase Petkoski ; Viktor K. Jirsa  

 Check for updates

*Chaos* 35, 013161 (2025)

<https://doi.org/10.1063/5.0158186>



### Articles You May Be Interested In

Propagation of spiking regularity and double coherence resonance in feedforward networks

*Chaos* (January 2012)

Distinct subtypes of inhibitory interneurons differentially promote the propagation of rate and temporal codes in the feedforward neural network

*Chaos* (May 2020)

Effects of topologies on signal propagation in feedforward networks

*Chaos* (January 2018)



Chaos

Special Topics Open  
for Submissions

[Learn More](#)

# Synchronization in spiking neural networks with short and long connections and time delays

Cite as: Chaos 35, 013161 (2025); doi: 10.1063/5.0158186

Submitted: 15 May 2023 · Accepted: 13 December 2024 ·

Published Online: 30 January 2025



View Online



Export Citation



CrossMark

Lionel Kusch,<sup>1</sup>  Martin Breyton,<sup>1,2</sup>  Damien Depannemaecker,<sup>1</sup>  Spase Petkoski,<sup>1</sup>  and Viktor K. Jirsa<sup>1,a)</sup> 

## AFFILIATIONS

<sup>1</sup>Institut de Neurosciences des Systèmes, Aix-Marseille University, INSERM, Marseille 13005, France

<sup>2</sup>Service de Pharmacologie Clinique et Pharmacovigilance, Assistance Publique des Hôpitaux de Marseille, Marseille 13005, France

**Note:** This paper is part of the Focus Issue on Disruption of Networks and System Dynamics.

**a)** Author to whom correspondence should be addressed: [viktor.jirsa@univ-amu.fr](mailto:viktor.jirsa@univ-amu.fr)

## ABSTRACT

Synchronization is fundamental for information processing in oscillatory brain networks and is strongly affected by time delays via signal propagation along long fibers. Their effect, however, is less evident in spiking neural networks given the discrete nature of spikes. To bridge the gap between these different modeling approaches, we study the synchronization conditions, dynamics underlying synchronization, and the role of the delay of a two-dimensional network model composed of adaptive exponential integrate-and-fire neurons. Through parameter exploration of neuronal and network properties, we map the synchronization behavior as a function of unidirectional long-range connection and the microscopic network properties and demonstrate that the principal network behaviors comprise standing or traveling waves of activity and depend on noise strength, E/I balance, and voltage adaptation, which are modulated by the delay of the long-range connection. Our results show the interplay of micro- (single neuron properties), meso- (connectivity and composition of the neuronal network), and macroscopic (long-range connectivity) parameters for the emergent spatiotemporal activity of the brain.

© 2025 Author(s). All article content, except where otherwise noted, is licensed under a Creative Commons Attribution-NonCommercial-NoDerivs 4.0 International (CC BY-NC-ND) license (<https://creativecommons.org/licenses/by-nc-nd/4.0/>). <https://doi.org/10.1063/5.0158186>

**The research highlights the significant impact of short-range and long-range connections on synchronization within spiking neural networks. By employing computational models, the study reveals that the delay along these connections plays a crucial role in modulating synchronization. This finding provides valuable insights on how structured activity emerges at different scales of brain organization. Furthermore, this provides an insight into the dynamics of synchronization in spiking neuronal networks and its dependence on various network properties, such as noise strength, balance between excitatory and inhibitory neurons, and voltage adaptation. Understanding these factors is essential for deciphering the complex spatiotemporal activity of the brain and understanding its dynamics, bridging the gap between different modeling approaches, and offering valuable insights about the behavior of spiking neural networks.**

## I. INTRODUCTION

Brain activity is characterized by rich spatiotemporal dynamics across scales. Among these, synchronization<sup>1</sup> between rhythms

of neuronal populations<sup>2</sup> has been shown to be relevant for brain function<sup>3</sup> and dysfunction.<sup>4</sup> Different spatial patterns of synchronization have been hallmarked both during tasks<sup>5</sup> and rest<sup>6,7</sup> and through various neuroimaging modalities such as functional Magnetic Resonance Imaging (fMRI), Magneto-Encephalography (MEG/EEG), and Electroencephalography (EEG). Similarly, neurons are known to synchronize locally through short-range connections, as seen in Local Field Potentials (LFPs), which also bear relevance for the brain function.<sup>8</sup> Hence, even if it is established that the macroscale rhythms emerge from the microscopic spiking neuronal activity,<sup>9,10</sup> the interplay between the two scales is often poorly understood.

Generative computational models have been commonly used<sup>11–14</sup> to understand how the brain's anatomical structure, as defined by its connectome,<sup>15</sup> impacts structured macroscopic patterns of brain activity. Here, we explore how these emergent dynamics depend not only on the weights of the connectome but also on the time it takes to propagate through the fibers.<sup>16–18</sup> Together, they define a space–time structure that is determinant for the network behavior, including resonance, synchronization, and emergence of brain rhythms.<sup>19</sup>

The space-invariant short-range cortical connections in the brain are characterized by negligible delays.<sup>13</sup> Alongside these are heterogeneous links from the connectome, distinguished by their time delays and weights.<sup>20</sup> To investigate the interplay between these two types of connections, this study simplifies the scenario by focusing on the impact of a single long-range link. Through systematic alteration of its length, and consequently its delay by keeping a constant transmission velocity, the study aims to elucidate the effects of these long-range connections on neural interactions.

The effects of network heterogeneity, including that of time delays, were studied on the macroscopic level,<sup>21–23</sup> as well as for the combined macro- and mesoscopic representations<sup>24–28</sup> using a neural field approach, including both global and local connectivities.<sup>13,29,30</sup> However, neural fields in those cases were either modeled by mean-field representations of the neuronal masses or by phenomenological neuronal models that correspond to reduced representations of Hodgkin–Huxley neurons. In the case of integrate-and-fire neuron models, there is a lack of a precise and self-consistent mathematical framework to link microscopic and macroscopic dynamics within neural field theory.<sup>31</sup> In particular, the validation of macroscopic phenomena emerging from spiking neuronal networks is missing.

In this study, we focus on the emergence of synchronization in neural fields coupled through long-range connections (LRCs) with finite transmission velocity.<sup>24,26,27,32–35</sup> We use a methodology similar to Jirsa and Stefanescu<sup>32</sup> but with a more detailed and physiologically grounded model of neurons including adaptation phenomena. This last aspect is critical since the previously used simpler neuron model embodied strong slow attractive manifolds known to be the key determinant in network synchronization. As a consequence, the synchronization results reported in the literature may not always translate into real-world brain networks.

To address this, we introduce a detailed description of the spiking network followed by a description of a reduced analytical model to capture the observed synchronization. In the results, we first present the effects of the LRC parameters and noise intensity on synchronization. Then, we explore the joint effects of neuron parameters (e.g., adaptation) and LRC delay on the modulation of synchronization. We then compare the spiking network and the analytical model, and finally, we describe the parameters (E/I balance, network size) that tend to break synchronization, always in relation to the LRC delay and the emergent dynamics.

## II. MODELING THE NETWORK OF NEURONS

### A. Network of spiking neurons

We consider a two-dimensional grid network consisting of 200 cells ( $10 \times 20$ ), each with a size of  $3 \times 3 \text{ mm}^2$ , and two boundaries with periodic conditions [see Fig. 1(a)] topologically equivalent to a torus. Neurons are distributed homogeneously on the grid with the only constraint that each cell contains a fixed number of excitatory (160) and inhibitory (40) neurons [see Fig. 1(b)], following the proportion observed in the cortex.<sup>36,37</sup> All neurons were constructed identically with an adaptive exponential integrate-and-fire model<sup>38</sup> with alpha conductance synapses without delay. Only the post-synaptic weights were different between excitatory and inhibitory

neurons. The following set of equations describes the network:

$$\begin{aligned} C_m \times \frac{dV_m}{dt} &= -g_L(V_m - E_L) + g_L \times \Delta_T \times e^{\frac{V_m - V_{th}}{\Delta_T}} \\ &\quad - g_e(t)(V_m - E_{ex}) - g_i(t)(V_m - E_{in}) \\ &\quad - w + I_e + \mathcal{N}(0.0, \sigma^2), \\ \tau_w \times \frac{dw}{dt} &= (a \times (V_m - E_L) - w), \\ g_e(t) &= \sum_{t_j^{(f)}} w_j \times \text{alpha}(t - t_j, \tau_{ex}) \text{ with } w_j > 0.0, \\ g_i(t) &= \sum_{t_j^{(f)}} w_j \times \text{alpha}(t - t_j, \tau_{in}) \text{ with } w_j < 0.0, \\ \text{alpha}(t, \tau) &= \frac{t}{\tau} \times e^{1 - \frac{t}{\tau}} \times \text{Heaviside}(t), \end{aligned}$$

where  $V_m$  is the membrane voltage,  $w$  the adaptation current,  $g_e$  the excitatory synaptic conductance, and  $g_i$  the inhibitory synaptic conductance of one neuron.  $t_j^{(f)}$  represents spike-time from pre-synaptic neurons. When the membrane potential crosses a threshold  $V_{peak}$ , the membrane voltage is reset ( $V_{reset}$ ), and the adaptive current is increased by a value  $b$  (for more detail, see Table II D in the [supplementary material](#)). Each neuron has two external inputs:  $I_e$ , corresponding to a constant external current, and  $\mathcal{N}$ , corresponding to white noise drive.  $I_e$  is set to 0.0 pA for all neurons when simulating a homogeneous population, but it follows a Gaussian distribution centered around zero when exploring the effect of heterogeneity of neurons. The refractory time is not an explicit parameter in the equations but is included in the simulator. It is a period during which the membrane potential of the neuron is clamped to its resting value, preventing it from generating a new spike. The initial condition is chosen so that the network is in an asynchronous irregular state when disconnected. The choice of the well-described adaptive exponential integrate-and-fire (AdEx) model<sup>38–41</sup> is motivated by its capability of reproducing most neural firing patterns.<sup>39,42</sup> Other models, such as conductance-based adaptive exponential model,<sup>43</sup> multi-timescale adaptive threshold model, and<sup>44</sup> generalize integrate-and-fire neuron<sup>45</sup> or Hodgkin–Huxley neurons,<sup>46</sup> also express this variety of dynamics, but they are harder to analyze in the case of our study, either due to a large number of parameters or to the lack of detailed characterization. On the contrary, models, such as leaky integrate and fire<sup>47,48</sup> or FitzHugh–Nagumo,<sup>49,50</sup> are simpler and have already been studied with a similar network topology<sup>32,51</sup> and do not have the same richness in term of dynamical repertoire as AdEx.

The neurons in the network are divided into excitatory (80%) and inhibitory (20%) based on the sign of their post-synaptic weights. Each neuron projects probabilistic short-range connections around it following a two-dimensional Gaussian distribution Fig. 1(d):

$$p(d_x, d_y) = e^{-\frac{(d_x - \mu_x)^2 - (d_y - \mu_y)^2}{2\sigma^2}},$$

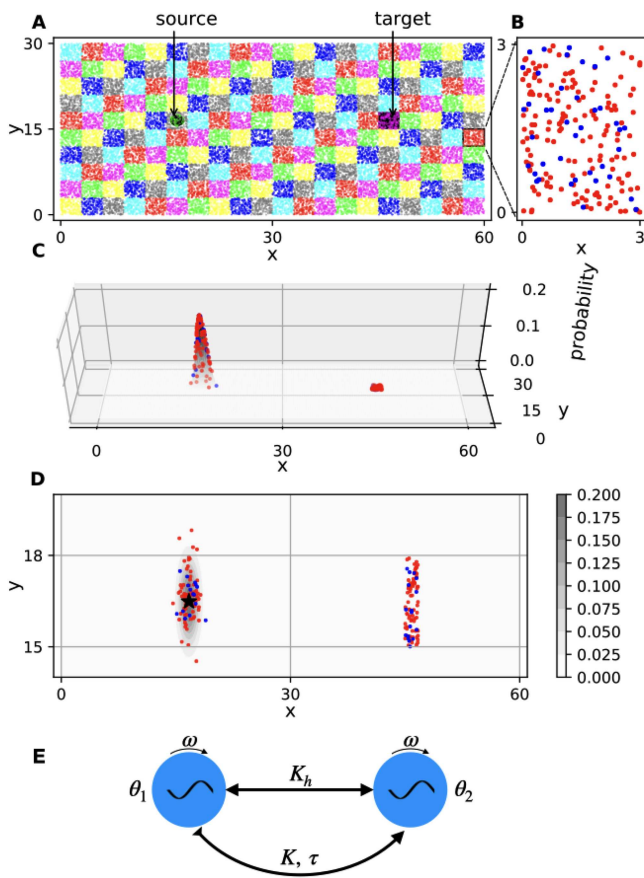


**FIG. 1.** Network topology. (a) The network topology is based on a two-dimensional grid network consisting of 200 cells ( $10 \times 20$ ), each with a size of  $3 \times 3 \text{ mm}^2$ . The black arrows represent the ends of the long-range connections between cells, with uni-directional connections from the center of the source cell to the target cell. (b) Each cell contains 140 excitatory neurons (red) and 60 inhibitory neurons (blue), randomly positioned. (c) An example distribution of post-synaptic neurons. On the left are the local connections to one pre-synaptic neuron. On the right, all the post-synaptic neurons connected to the source cell through the LRC. Excitatory neurons are colored in red, and inhibitory neurons in blue. (d) is the projection of (c) on the torus surface. The gray scale is the two-dimensional Gaussian probability of local connections with the position of the pre-synaptic neuron represented by the black star. The probability function on the target of the LRC is not shown. (e) A sketch of the approximation of the full network synchronized activity with two coupled phase oscillators.

where  $(d_x, d_y)$  is the distance along the x and y axes between two neurons and  $m_x$  and  $m_y$  are their position on the grid. Projections of the excitatory neurons decay faster ( $\sigma = 0.8$ ) than those of inhibitory neurons ( $\sigma = 1.2$ )<sup>32</sup> see Fig. 1(c)]. To achieve an asynchronous irregular state<sup>52</sup> in a noise-driven balanced network of neurons, the weight of the excitatory synapses was set to 10.0 nS and the ratio (excitatory/inhibitory) to 0.11 after parameter explorations.

The LRC is defined by a source cell and a target cell. In the source cell, on top of the short-range connections, 40% of the

excitatory neurons project to the distant target following a two-dimensional Gaussian probability density ( $\sigma_{long} = 2.0$ ) [see Figs. 1(c) and 1(d)] centered in the target cell. The weight of the LRC is independent of the local ones (by default: 15.0 nS), and their delay is uniform between neurons and independent of the distance.

The synchronization of the network due to LRC is quantified using the coefficient of variation of the firing rate (FR), as proposed by Brunel.<sup>52</sup> This metric is calculated by dividing the standard deviation of the firing rate (number of spikes per time bin of 3 ms) by its mean throughout 10 s,

$$CV_{FR} = \frac{\sigma_{FR}}{\mu_{FR}}.$$

A  $CV_{FR}$  value higher than 1.0 between two neurons indicates that they are synchronized and asynchronous otherwise. To reduce the bias induced by initial conditions, an initial transient period of 12 s is discarded in each simulation that is run only once for a specific parameter set.

Another quantification of the synchronization is based on the Kuramoto order-parameter.<sup>53</sup> Kuramoto introduced a model to describe and analyze the synchronization of coupled intrinsic oscillators,<sup>53</sup> each described by the following equation:

$$\dot{\theta}_i = \omega_i + \frac{K}{N} \sum_{j=1}^N \sin(\theta_j - \theta_i), \quad i = 1 \dots N,$$

for a system composed of  $N$  limit-cycle oscillators, with phases  $\theta_i$  and a coupling factor  $K$  between them.

This model of oscillators can be applied to neurons by considering that a phase reset occurs at every spike and that the phase increases linearly between spikes.<sup>54</sup> The instantaneous phase then becomes proportional to the time elapsed between two spikes,

$$\psi(t) = 2\pi m + 2\pi \frac{t - t_m}{t_{m+1} - t_m}, \quad \forall t \in [t_m, t_{m+1}],$$

where  $m$  is the spike index and  $t_m$  the time when the  $m$ th spike occurs. The synchronization of the population can then be quantified by the absolute value of the complex Kuramoto order-parameter defined by the absolute value of the mean phase across neurons,

$$Re^{i\psi} = \frac{1}{N} \sum_{j=1}^N e^{i\theta_j}.$$

For the case of pairwise synchronization, a commonly used metric is the Phase Locking Value (PLV),<sup>23,55</sup> which is a statistical measure for similarity between phases of two signals, and is defined as

$$cPLV_{ij} \equiv PLV_{ij} e^{i\Delta\theta_{ij}} = \frac{1}{M} \sum_{m=1}^M e^{i\Delta\theta_{ij}(m)}, \quad (1)$$

where the phase difference  $\Delta\theta_{ij}(m) = \theta_i(m) - \theta_j(m)$  is calculated at times  $m = 1 \dots M$ . We used this metric to recover the synchronization,  $PLV = |cPLV|$ , and the phase difference  $\Delta\theta = \text{angle}(cPLV)$  for the analytical model with two coupled oscillators.

### B. Mathematical model of the spiking network

Given the topology of the system under study, for the cases when the network is synchronized, we propose to approximate this spiking neural network by two oscillators (each representing one half of the torus) coupled through one local bidirectional connection that takes into account the homogeneous local connectivity in the network and one uni-directional link corresponding to the LRC. Based on the Kuramoto model,<sup>53</sup> we arrive with the following coupled differential equations to describe the dynamics of each oscillator:

$$\dot{\theta}_1 = \omega - K_h \sin(\theta_1 - \theta_2), \tag{2a}$$

$$\dot{\theta}_2 = \omega - K_h \sin(\theta_2 - \theta_1) - K \sin(\theta_2 - \theta_1(t - \tau)). \tag{2b}$$

The first equation represents the half of the torus which is the source of the LRC. This oscillator with natural frequency  $\omega$  is coupled to the other oscillator only by the local homogeneous connections through the torus surface with a homogeneous coupling weight  $K_h$ . The second equation models the second half of the torus which corresponds to the target of the LRC. It has the same natural frequency  $\omega$  and the same bi-directional coupling parameters  $K_h$  due to the homogeneity of the neurons and their connectivity on the torus. In this equation, there is an additional coupling term corresponding to the uni-directional LRC. This long-range coupling has a specific weight  $K$  and depends on the phase of the first oscillator after a time delay  $\tau$ .

To solve the equations for parameters  $\omega$ ,  $K_h$ , and  $K$ , we follow the assumption that there is always some levels of synchronization between the two populations of neurons and, therefore,

$$\dot{\theta}_1 = \dot{\theta}_2 = \Omega, \tag{3a}$$

$$\theta_1(t - \tau) = \theta_1(t) - \tau\Omega. \tag{3b}$$

By substituting the definitions of  $\dot{\theta}_1$  and  $\dot{\theta}_2$  in the previous system, we find that when  $\tau = 0$  this leads to

$$\omega = \Omega_{\tau=0} = \Omega_0. \tag{4}$$

Next, for any  $\tau$ , it holds that

$$\omega + K_h \sin(\Delta\theta) = \Omega, \tag{5a}$$

$$\omega - K_h \sin(\Delta\theta) - K \sin(\Delta\theta + \Omega\tau) = \Omega, \tag{5b}$$

where  $\Delta\theta$  is the phase difference between the two oscillators. This yields

$$\omega = \Omega_0, \tag{6a}$$

$$K_h = \frac{\Omega - \omega}{\sin(\Delta\theta)}, \tag{6b}$$

$$K = -\frac{2 * (\Omega - \omega)}{\sin(\Delta\theta + \Omega\tau)}. \tag{6c}$$

Here,  $\omega$  was set by measuring the natural oscillation frequency of the network in the absence of any LRC. We then selected some data generated by the spiking network under the following parameters:  $Q_{long} = 10$  nS,  $Q_e = 10$  nS,  $Q_i = 11.0$  nS,  $\tau_{long} = [0.0, 200$  ms],

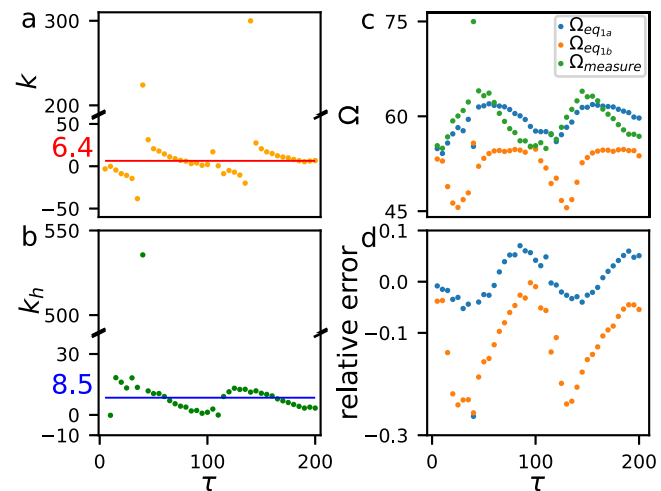


**FIG. 2.** Parameter fitting of the oscillator model (a) and (b) show the values of  $K$  and  $K_h$  obtained by injecting values of  $\Omega$ ,  $\omega$ , and  $\Delta\theta$  measured in the spiking network for different values of  $\tau$  into Eqs. (6c) and (6b). The horizontal lines correspond to the median values of  $K$  and  $K_h$ . (c) presents the values of  $\Omega$  measured in the spiking network for different  $\tau$  ( $\Omega_{measured}$ ) and the recalculated values from Eqs. (3a) ( $\Omega_{eq1a}$ ) and (3b) ( $\Omega_{eq1b}$ ) using the selected median  $K$  and  $K_h$ . (d) shows relative errors between the theoretical values and the measures [from (3a) in blue and from (3b) in orange].

$a = 0.0$  nS,  $I = 0.0$  nS. For each value of  $\tau \in [0 - 200$  ms], we extracted  $\Delta\theta$  and  $\Omega$  from the data to calculate the values of  $K_h$  and  $K$  (the values in Fig. 2) and selected the median values for the rest of the analysis. We also recalculated the theoretical values of  $\Omega$  from Eqs. (5a) and (5b) for the recovered  $K_h$  and  $K$  and compared them with the measured values in Fig. 2.

In addition, we used this theoretical model to check for co-existence of multiple stable solutions for  $\Omega$ , as it is common in delay-coupled phase oscillators.<sup>23,56-58</sup> To do so, we solved geometrically the system of transcendental Eqs. (5a) and (5b) for the recovered  $K_h$  and  $K$ , where the frequency of synchronization in our system is confined in the interval  $[\omega - k_h, \omega + k_h]$ , as a consequence of (5a). Next, we calculated the linear stability of the observed solutions by determining the largest real eigenvalue of the Jacobian of the system.

### III. RESULTS

We seek to recover and understand the conditions in which the network of spiking neurons is synchronized and to characterize its spatiotemporal dynamics, particularly with respect to the long-range connection. To this end, we conducted analyses of parameter spaces of synchronization as a function of global and local network parameters, i.e., weight and delay of unidirectional LRC for the former, and excitatory weights and variance of white noise for the latter.

Overall, time series analysis reveals that different levels of synchronization are associated with specific spatiotemporal patterns of activity. When the network is asynchronous [Fig. 3(a), corresponding to mark A in Fig. 4(b)], the activity corresponds to

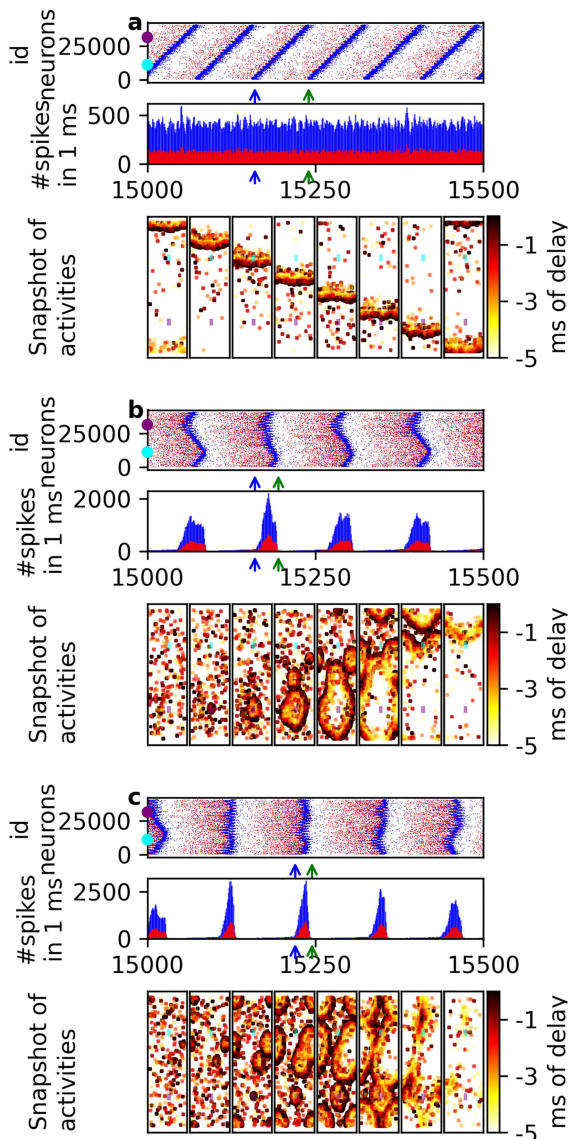


**FIG. 3.** Three characteristic network dynamics. A network of 40 000 neurons was simulated with white noise, synaptic weights of 10 nS, and different delays of the uni-directional long-range connections [(a) 40 ms, (b) 80 ms, and (c) 100 ms]. The index is ordered by cells of the grid, with excitatory neurons followed by inhibitory neurons. Each simulation is represented by spike trains and an associated histogram (bin: 1 ms) between 15.0 and 15.5 s. The blue and green arrows indicate the eight regular snapshots' start and end. On the histogram and eight snapshots, blue and purple represent the source and the target population. (a) Traveling wave; (b) regular bump from the target population with some other bumps; and (c) multiple bumps at the time.

a traveling wave along the longest axis of the grid. As expected, the histogram is flat, and the spike trains form a diagonal of spikes due to the ordering of the neurons. In contrast, when the network is highly synchronized [Fig. 3(c) corresponding to mark C in Fig. 4(b)], its

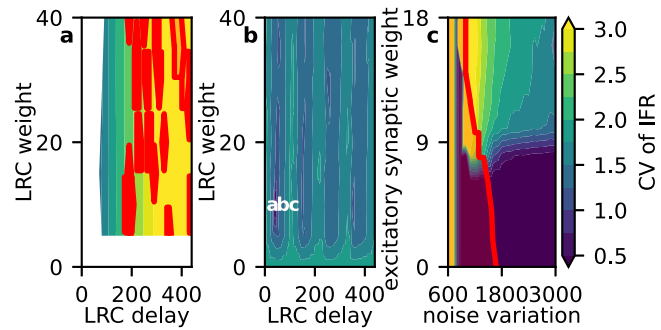


**FIG. 4.** Effects of excitation (short and long range) and noise on synchronization. Network synchronization is measured by  $CV_{FR}$  (window of 3 ms, no overlap) over 10 s of activity. (a) and (b) show the parameter space analysis of  $CV_{FR}$  for different delays and weights of the LRC, without and with noise (1800 pA), respectively. The white area in (a) corresponds to silent activity where no spikes occur. (c) displays the  $CV_{FR}$  for increasing noise intensity and excitatory synaptic weights in the absence of LRC. The parameters chosen for the simulations are shown in Fig. 3 as indicated by (a), (b), and (c).

activity alternates between bursts of activation and quiet periods. In this case, activity bursts are very short (less than 20 ms) and composed of multiple bumps (locally synchronized firing of neurons) mainly starting from the target cell, but also from other random locations due to the noise. The eight snapshots indicate that when two waves collide, they collapse. Between these two extremes, spatiotemporal patterns present a gradient where synchronization is linked to shorter activity bursts (on the scale of the whole network) and a higher number of bumps from random locations [see Fig. 3(b) corresponding to mark B in Fig. 4(b)].

### A. Independent contributions of LRC and noise

When the noise is turned off, the network is generally highly synchronized, as shown by the coefficient of variation being systematically higher than 1.0 [Fig. 4(a)]. Time series (Fig. S1 in the supplementary material) are characterized by periodic bumps starting from the target cell, forming a circular wave, and eventually colliding with itself. We find an almost proportional relationship between the level of synchronization and the delay. This relation is preserved when the weight of the LRC, the number of connections, and the position of the target cell are varied. However, the network is silent when the LRC weight is less than 5 nS, when the delay is less than 70 ms, or when the standard deviation of the Gaussian kernel is lower than 0.5.

When the LRC are removed, the parameter space [Fig. 4(c)] shows that the network is synchronized only when the noise is strong enough (variance greater than 1500 pA) and if the excitatory synaptic weight is sufficiently large (higher than 8 nS). When these conditions are met, synchronization decreases as noise increases with little effect of excitatory synaptic weights. A related phenomenon to this is the appearance of synchronized bumps displaying chaotic-like behavior<sup>59</sup> (see Figs. S2A and S2B in the supplementary material). When the excitatory synaptic weight is

too low, below 8 nS, the system remains in an asynchronous regime (Fig. S2 in the [supplementary material](#)).

### B. Synergic effect of LRC and noise

Under the combination of noise and the presence of LRC, the results show that the level of synchronization depends on the delay along the LRC [Fig. 4(b)], with a regular pattern of higher synchronization occurring at 0, 110, 220, or 330 ms. This indicates inherent oscillations with a period of 110 ms. The observed impact of the delay on synchronization is similar to the one found in populations of oscillators.<sup>56,60</sup> The same effect was also observed for continuous spiking neurons.<sup>32</sup>

If the weight of the LRC or the number of connections is too low, this effect is lost, and the network remains synchronized regardless of the delay. Like before, we found that the position of the target cell does not have a substantial impact on synchronization. In other words, if the contribution of the LRC is too small, then the noise is the dominant cause for the emergence of synchronized activity, Figs. 4(b) and 4(c). Otherwise, LRC modulates synchronization through the ratio between the delay and mean firing rate, determining the increased/decreased synchronization ranges.

When the synchronization is facilitated, e.g., point C in Fig. 4(b), the wave is homotopic and propagates faster [Fig. 3(b) compared to Fig. 3(c)], compared to the case when the synchronization is decreased, e.g., point B in Fig. 4(b). In certain conditions, point A in Fig. 4(b), regular traveling waves appear. In this case, the source and the target cells are anti-phase (close to half of the period), and the bump does not collapse but continues to travel across the network.

### C. Modulation by adaptation current

The adaptive current is a mechanism that affects the frequency of the spikes. When adaptation parameters increase, new spikes are harder to trigger so neurons receive less input from their neighbors. This impacts the mean-firing rate, which serves as a “natural frequency” of self-sustained network oscillations in the case of synchronization, ultimately leading to a similar effect in synchronized oscillators as reducing the time delays (Fig. 5).

The adaptation has three main parameters: the time constant  $\tau_w$ , the spike-triggered adaptation  $b$ , and the sub-threshold adaptation  $a$ . As seen in Fig. 5, synchronization can be found for all ranges of these parameters. The periodic effect of the LRC delay on synchronization found previously is preserved when adaptation is varied but tends to fade out as the adaptation increases. The spike-triggered adaptation and the time constant are associated with a gradient of  $CV_{FR}$ , not found with subthreshold adaptation. Low values of  $\tau_w$  and  $b$  induce an increase of the mean firing rate.  $a$  also impacts firing rate but to a lesser degree (details in Fig. S3 in the [supplementary material](#)).

### D. Effect of excitability of the voltage membrane

We applied heterogeneous external currents,  $I_e$ , distributed across neurons, to create heterogeneity of excitability within the population (see Sec. II). The voltage membrane excitability has opposite effects on adaptation as it facilitates the generation of

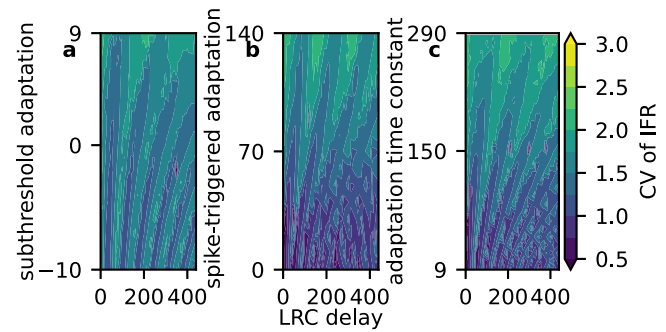


**FIG. 5.** Effects of different properties of current adaptation and LRC delay on network synchronization. Network synchronization is quantified by  $CV_{FR}$  (a window of 3 ms, no overlap) over 10 s of activity. The parameter spaces presented show the relationship between the LRC delay and the properties of current adaptation of the neurons, including sub-threshold adaptation (a), spike-triggered adaptation (b), and adaptation time current (c).

spikes. Therefore, as seen in Fig. 6(a), increasing heterogeneity tends to reduce the  $CV_{FR}$  and the periodic effect of the delay also fades out for low values, mirroring the effect of adaptation. Although not presented here, if heterogeneity is too extreme, it affects the balance of the network and pushes it into an asynchronous irregular state. The relationship between voltage reset and firing rate can be found in Fig. S7 in the [supplementary material](#).

Synchronization is mainly present for a voltage reset between  $-63$  and  $-45$  mV [see Fig. 6(b)], otherwise the network is mostly asynchronous. In the bottom part of the panel, there is almost no activity in the network (close to zero mean firing rate and CV, Figs. S11E and S11F in the [supplementary material](#)) except for some high-frequency bursts for specific values of the LRC delay, yielding narrow stripes of synchronized activity. This separation between synchronous and asynchronous regimes may be explained by a strong non-linear relationship between the mean firing rate and the voltage reset (Fig. S4D in the [supplementary material](#)).

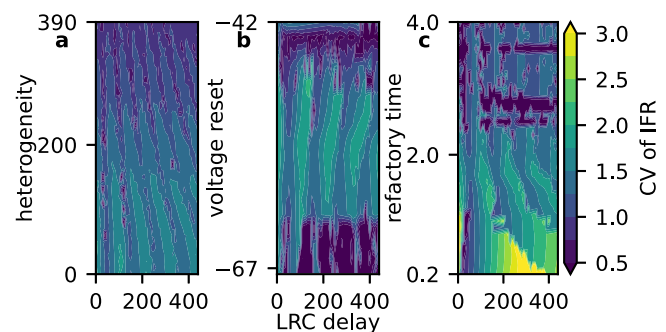


**FIG. 6.** Effects of different membrane voltage properties LRC delay on network synchronization. Network synchronization is quantified by  $CV_{FR}$  (a window of 3 ms, no overlap) over 10 s of activity. The parameter spaces presented show the relationship between the LRC delay and the voltage membrane properties of neurons, including heterogeneity (a), voltage reset (b), and refractory time (c).



When the refractory time is varied [Fig. 6(c)], the parameter space is separable in two subspaces: under and over 1.7 ms, approximately. For low refractory times, more than 95% of the neurons have irregular burst activities (Fig. S7 in the [supplementary material](#)). In this case, reducing refractory time increases the variation of the  $CV_{FR}$  proportionally to the delay. However, large values of  $CV_{FR}$  (above 3) capture the presence of large waves (see Fig. S5A in the [supplementary material](#)). When the refractory period exceeds 1.7 ms, neurons regularly spike with few bursts with little to no effect of the delay along the LRC. In this scenario, very low values of CV (below 0.5) capture traveling wave activity (shown in Fig. S5C in the [supplementary material](#)).

### E. Comparison with the approximation of two phase oscillators

In this section, we compare synchronization results obtained in the spiking network and the analytical model derived for two uni-directionally delay-coupled phase oscillators. We now characterize the synchronization for the spiking neurons using the Kuramoto order parameter ( $R$ ) instead of the  $CV_{FR}$ , while for the pairwise coherence of the phase oscillators, we use the absolute value of the phase locking value (PLV). Specifically, we select [Figs. 7(a)–7(c)] the LRC weight, sub-threshold adaptation, and heterogeneity between neurons for a range of the LRC delay as the parameters to be compared with  $K$ ,  $\omega$ ,  $K_h$ , and  $\tau$  of the analytical model [Figs. 7(d)–7(f)]. We find that the model of phase oscillators consistently reproduces the activity of the spiking neuronal network. The weight of the LRC has the same effect on synchronization in the network as  $K$  (long-range coupling) between the oscillators, despite the changes in the frequency of synchronization. The pattern of synchronization found when varying the sub-threshold adaptation parameter is also retrieved when decreasing the natural frequency ( $\omega$ ) of the oscillators. Lastly, decreasing the heterogeneity of the neurons in the network tends to facilitate synchronization by increasing the probability of simultaneously having a greater number of neurons close to the firing threshold. Hence, this has the same effect as increasing the local coupling  $K_h$  that also brings neurons closer to synchrony and we find a similar pattern of synchronization for different values of  $\tau$ .

Additionally, solving geometrically the system of transcendental Eqs. (5a) and (5b) for the recovered values of  $K_h$  and  $K$ , allowed us to calculate the linear stability of the observed solutions. Even though we observed a small range in the values of  $\tau$  where two stable fixed points coexist (see Fig. S6A and S6B in the [supplementary material](#)), we always observed only one of them in the numerical simulations of the phase oscillators. It is, thus, likely that this co-existence is a numerical artifact of the method for geometrically solving the transcendental equations since the range of co-existence is within the margins of the numerical error for the solver. However, another possibility is that the other solution was not observed because it is less stable than the one that was observed (see Fig. S6C in the [supplementary material](#)).

### F. Network effects: Balanced network

As seen in previous studies,<sup>61</sup> synchronizations occurs in a network of spiking neurons for a specific balance between excitation

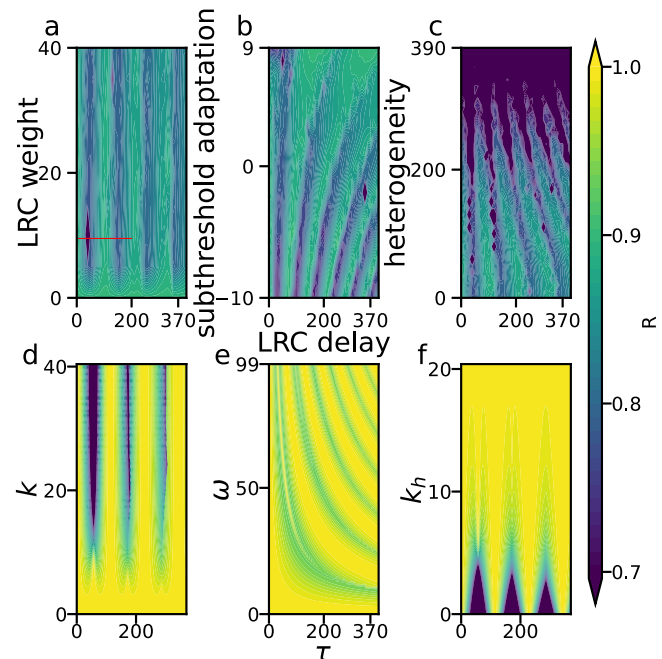


**FIG. 7.** Kuramoto synchronization of the spiking network and the oscillator model. (a), (b), and (c) are the results from the spiking networks, measured by the Kuramoto order parameter, varying the LRC weight, sub-threshold adaptation, and heterogeneity of neurons for different values of the LRC delay. In (a), the red line points to the range of data used for solving the analytical model. (d), (e), and (f) present synchronization results between the two oscillators of the analytical model varying  $K$ ,  $K_h$ ,  $\omega$ , and  $\tau$ .

and inhibition that allows for wave propagation. Other factors, such as the number of neurons and the synaptic weights also affect network synchronization.<sup>32</sup> Plots in Fig. 8 show the effect of the relative strength between excitatory and inhibitory synaptic weights on synchronization for different noise intensities (0, 1800, and 2600 pA). Without noise, only the LRC delay has a significant effect on synchronization, similarly to the previous results of Fig. 4 with the same characteristic proportional relationship. The main difference is that for a low E/I ratio (approximately under 0.06) asynchronous activity is seen [but no activity at all for low  $k$  in the plot (a)]. This regime is also independent of noise intensity and simulations always have a firing rate over 50 Hz.

When noise is introduced, there appears a specific range of E/I balance that generates synchronization and the parameter space is divided into two regimes: one asynchronous regime, either dominated by excitation (top) or by inhibition (bottom), and a synchronized “balanced” regime in the middle.<sup>62,63</sup> The increase in noise intensity narrows this range of synchronization by pushing the upper limit down to a lower E/I balance.

### G. Network effects: Network size

To explore the effect of the number of neurons on synchronization, we varied the percentage of active neurons in the network. As

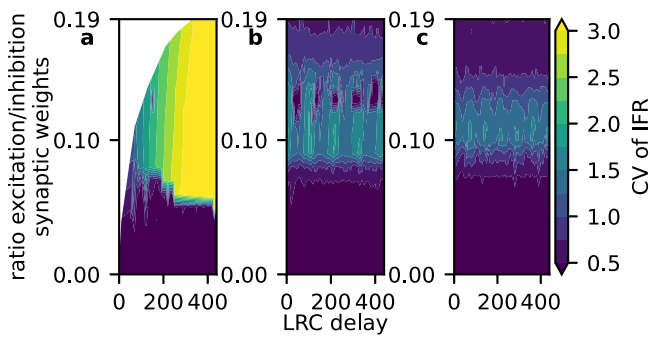


**FIG. 8.** Network synchronization analysis of ratio excitatory/inhibitory synaptic weight in relation to the LRC delay for different values of noise. Network synchronization is quantified by  $CV_{FR}$  (window of 3 ms, no overlap) over 10 s of activity. The three panels correspond to different values of noise: 0.0 pA in (a); 1800.0 pA in (b); and 2600.0 pA in (c).

seen from left to right in Fig. 9, the sparsening of neurons is associated with an increase in the lower bound of excitatory synaptic weights needed to reach synchronization. However, when the number of neurons is too low [plot (d)] increasing excitation can no longer compensate for the loss of activity. This balance between the number of neurons and excitatory synaptic weights is also reflected in the firing rate as the increase of synaptic weights can compensate for the reduction in the number of neurons to keep it constant<sup>64</sup> (Fig. S8 in the [supplementary material](#)).

In addition, we explored different grid sizes without changing the density of the neurons and found invariant results except for very small grids (less than five cells) (see Fig. S14 in the [supplementary material](#)).

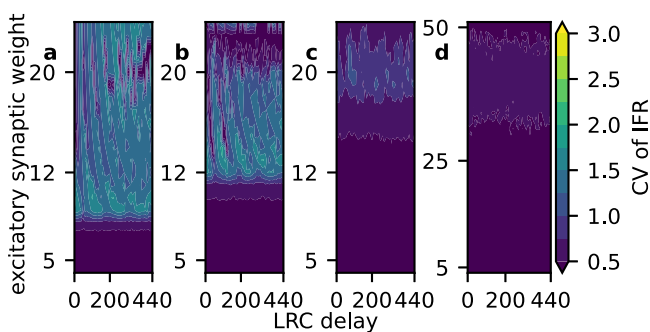


**FIG. 9.** Effects of synaptic weights and LRC delay of network synchronization for different sizes of the network. Network synchronization is quantified by  $CV_{FR}$  (a window of 3 ms, no overlap) over 10 s of activity. The parameter spaces presented show the relationship between the delay of the long-range connection and the synaptic weight for different percentages of active neurons [(a) 100%, (b) 75%, (c) 50%, and (d) 25%].

## H. Topology effects: Bi-directional long-range connections

In the previously shown results with unidirectional LRC [see Figs. S10A and 4(b)], varying the weights had very little or no effect on the synchronization for any fixed delay. However, when the LRC becomes bidirectional, synchronization is lost for LRC weights higher than 4 nS (Fig. S10B in the [supplementary material](#)).

In the absence of synchronization, activity resembles that of Fig. 3(a) with an unstable traveling wave across the network. When tuned near synchronization, we again find bumps of activity, but this time originating from both sides of the LRC, Figs. S12B and S12C in the [supplementary material](#). If the weight of the LRC is increased above 4 nS (from point C to D in Fig. S10C in the [supplementary material](#)), bumps of activation appear with origins alternating between both ends of the LRC, with roughly one-third of them never propagating through the network. The principal cause of the disappearance of the periodic dependence on the delay in the case of bidirectional LRC is that regardless of the noise level, the network is not synchronized. Still, a traveling wave occurs (see Fig. S9A in the [supplementary material](#)), while the same condition for a unidirectional LRC would have caused synchronization instead (see Fig. S9B in the [supplementary material](#)).

## IV. DISCUSSION

The present study demonstrates the conditions necessary for synchronization in a two-dimensional surface comprised of adaptive exponential integrate-and-fire neurons,<sup>38</sup> incorporating long-range connections (LRC) with transmission delays. In particular, we have identified how the global synchronization is affected by the delay along the LRC. This relationship typically follows a regular pattern, contingent upon other parameters that we have examined. These results align with earlier works, confirming this phenomenon in a neural field derived from spiking neural networks,<sup>32</sup> as well as with broader literature illustrating Arnold's tongues for synchronization.<sup>65</sup> This relationship is contingent upon the ratio between natural frequencies and time delays.<sup>22,56</sup> Based on the latter, we also introduced a reduced analytical model. Besides its simplicity, it omits all the higher-order terms in the Fourier series of the phase-interaction function, and it still qualitatively captures and describes the observed synchronization phenomena, thus strengthening the validity of the numerically observed results.

We identified four key conditions that influence synchronization modulation by the LRC in the network. First, the network with LRC naturally tends to synchronize at a frequency that is dependent on the delay along the LRC. Adding an external input (here in the form of random noise) is also crucial for achieving synchronization and revealing a more intricate relationship between synchronization and delay. Second, the LRC must be sufficiently strong (measured by the weight and width of the kernel) to affect the network. However, synchronization no longer occurs if the LRC are bidirectional and their influence is too strong. The third condition is that the network must maintain a balance between inhibition and excitation<sup>61–63</sup> for the LRC to modulate the synchronization effectively. Finally, the number of neurons must be large enough<sup>34</sup> or sufficiently interconnected for this phenomenon to take place.

Through investigating the parameters space, we have done thorough parametrizations that correspond to various neuron subtypes. We started with values corresponding to adapting neurons in sub-threshold activities.<sup>42</sup> It corresponds to type II neuron models (as shown in Fig. S4C in the [supplementary material](#)) exhibiting resonator regimes<sup>39</sup> and type I Phase Response Curve (PRC).<sup>41</sup> When modifying neuronal properties, we changed firing rate dynamics, neuron type (I/II), voltage membrane regime, and PRC (as shown in Figs. S4 and S17 in the [supplementary material](#)). For instance, when the sub-threshold is shifted to low values, the adapting neuron in sub-threshold activities becomes a type I neuron with integrator regimes. Interestingly, we found that the type of neuron is not a significant condition for the effect of the LRC on synchronization. Moreover, when setting the spike-triggered adaptation to 0 pA, the neuron model becomes equivalent to an exponential integrate-and-fire neuron without adaptation. We observed that the results remain consistent for this neuron type as well. This indicates that mean field models derived from various neuron types would still conform to our findings. Additionally, considering that for every delay value along the LRC, there exists at least one set of neuron parameters (i.e., a neuron type) enabling network synchronization, it would be possible to deduce neuron properties from knowledge about the LRC, under certain conditions about the spiking activity.

In terms of generative mechanisms, we identified that the bumps are the main cause of synchronization captured by the coefficient of variation of the firing rate  $CV_{FR}$ , and that the bumps correspond to a burst of activity where many neurons are collectively triggered in a short period of time. These bursts are generated periodically and their generative process resembles the one of action potentials by following a sequence of voltage accumulation, threshold crossing, spike triggering, and a refractory period. When the noise drive is high enough to trigger a spike at the single neuron level, the synaptic currents will accumulate locally through the synaptic weights (mediated by the local E/I balance). If the local voltage becomes large enough, it generates circular waves that propagate through the network. In the case of a homogeneous network, the probability of these events forming anywhere on the grid is uniform, potentially generating multiple waves from different locations at the same time. The collapsing of waves is followed by a silent period due to the refractory time ensuing collective firing of neurons. Indeed, the local increase of adaptation current prevents neurons from generating new spikes. The adaptation current then decays until new events occur. As a result, the frequency of bursts depends on a complex interaction between the adaptive current, synaptic current, voltage reset, refractory time, E/I balance, and noise.

Finally, the characteristics of both, neurons and the network, influence how emergent phenomena like synchronization and waves develop as spatiotemporal patterns in the population. This study establishes connections between these emergent dynamics and the properties of long-range fiber-like connections. Understanding and describing this self-organization is crucial for understanding complex systems like the brain. In particular, both the delay and the weights of the fibers play crucial roles in network synchronization, alongside neuronal properties. Specifically, variations in adaptive current and voltage reset can affect the synchronization of certain neurons, impacting the emergent rhythm of the neuronal population.<sup>66</sup> Furthermore, wave propagation, as demonstrated in

this study, is crucial for synchronization as an emergent dynamic. Our results corroborate previous findings by showing that local modifications such as a change in the E/I balance or a loss of neurons can disrupt higher-order phenomena (e.g., wave propagation and synchronization) and, thus, could potentially be responsible for altered brain activity observed in pathology.

One major limitation of our work lies in the choice of the synchronization metrics. Here, synchronization is quantified using the coefficient of variation of firing rate ( $CV_{FR}$ ), which is less precise in the case of bursts (the cause of variation can be the high activities of a sub-population). Nevertheless, we were able to reproduce some of the main results using the time-averaged Kuramoto order-parameter,<sup>53</sup> when we compared the analytical model to the network activity. The time-averaged Kuramoto order-parameter has the particularity to be robust to the bursting effect, as shown by Borges *et al.*<sup>54</sup> Finally, for the analytical model, a better fit would have been obtained by a more detailed model containing higher-order terms in the Fourier series of the coupling function.<sup>67</sup> Together with the higher-order network interactions<sup>68</sup> these play an important role in brain activity,<sup>69,70</sup> but the current parsimonious parametrization strengthens the universality of the observed phenomena.

Among other limitations, we can note that each network configuration was only tested once, thus bringing nuances to the conclusions that can be drawn about multiple regimes potentially coexisting for the same set of parameters. Indeed, some simulations showed transitions between regimes (see Fig. S13 in the [supplementary material](#)), making it difficult to determine if the simulation represents a complete stationary regime or only one regime in a more complex landscape. However, simulations were run long enough to reach a steady regime whenever it existed. Moreover, the analysis and especially the simulations of the reduced model did not give a strong indication for the coexistence of different solutions, and hence we did not pursue a more thorough exploration of dynamical regimes, since it would have been tedious and beyond the focus of this study.

Lastly, the analysis was not fully exhaustive; synaptic parameters such as Gaussian connectivity profiles,<sup>71</sup> time-constants, or reversal potentials, for example, were not explored because we chose to focus on neuronal properties important for mean field derivations.

In summary, the synchronization of a network of biological neurons with long-range connections and finite transmission velocities is modulated by the delay of these connections. The main conditions for this effect are the pre-existence of spontaneous activity driven by an external input (or noise), a significant contribution of the LRC, a balanced network (excitation/inhibition), and a large number of neurons. Given that our objective was to provide evidence for the validity of neural field models, future work could include testing the relaxation of neural field model assumptions (e.g., plasticity, delays, and weight distributions) and using multiple heterogeneous neuron models. Additionally, further analysis with bidirectional LRC is needed to understand spatiotemporal patterns in this case. This analysis should consider larger grids or modified connectivity, as recent findings suggest that traveling waves are based on a fraction of neurons in a population.<sup>66</sup> Validation of this phenomenon with more recent neural field models (e.g., Zerlaut *et al.*<sup>72</sup> or Augustin *et al.*<sup>73</sup>) is also recommended.

## SUPPLEMENTARY MATERIAL

See the [supplementary material](#) for additional information about other network metrics that we provide in open-source databases and details of the network simulation for the reproducibility of the results. The two supplementary notes describe the databases and the additional metrics applied to the network. The supplementary table is based on the proposition of a table by Nordlie *et al.*<sup>74</sup> for the reproducibility of the neural network model. The figures show the network topology, selection of different time series, and parameter explorations with selected additional metrics.

## ACKNOWLEDGMENTS

We acknowledge the use of Fenix Infrastructure resources, which are partially funded by the European Union's Horizon 2020 Research and Innovation Programme through the ICEI project under Grant Agreement No. 800858. This research has received funding from the European Union's Horizon 2020 Framework Programme for Research and Innovation under the Specific Grant Agreement Nos. 945539 (Human Brain Project SGA3), 101147319 (EBRAINS 2.0 Project), and 101137289 (Virtual Brain Twin Project), by the French government grant managed by the Agence Nationale de la Recherche (ANR) Reference No. ANR-22-PESN-0012 (France 2030 program), and from the ANR under Grant No. ANR-17-CE37-0001-CONNECTOME. The authors gratefully acknowledge the support team of the supercomputer Piz Daint at CSCS—Swiss National Supercomputing Centre.

## AUTHOR DECLARATIONS

### Conflict of Interest

The authors have no conflicts to disclose.

### Author Contributions

Spase Petkoski and Viktor K. Jirsa contributed equally to this work as the last author.

**Lionel Kusch:** Conceptualization (equal); Data curation (equal); Formal analysis (equal); Investigation (equal); Methodology (equal); Software (equal); Validation (equal); Visualization (equal); Writing – original draft (equal); Writing – review & editing (equal). **Martin Breyton:** Writing – original draft (equal); Writing – review & editing (equal). **Damien Depannemaecker:** Investigation (supporting); Methodology (supporting); Writing – review & editing (equal). **Spase Petkoski:** Conceptualization (equal); Formal analysis (lead); Investigation (lead); Methodology (lead); Project administration (equal); Supervision (equal); Writing – original draft (equal); Writing – review & editing (equal). **Viktor K. Jirsa:** Conceptualization (equal); Formal analysis (equal); Funding acquisition (lead); Investigation (equal); Methodology (equal); Project administration (lead); Resources (equal); Writing – original draft (equal); Writing – review & editing (equal).

## DATA AVAILABILITY

The code for the simulation and analysis of this paper is freely available under v2 Apache license at [https://bitbucket.org/lionekusch/torus\\_long\\_range\\_connection/src/paper/](https://bitbucket.org/lionekusch/torus_long_range_connection/src/paper/). Each exploration's

analysis results are registered in databases available on Zenodo (<http://dx.doi.org/10.5281/zenodo.7629156>) with the associate code. [Supplementary material](#) Note 1 describes the contents of them.

## REFERENCES

- <sup>1</sup>F. Varela, J.-P. Lachaux, E. Rodriguez, and J. Martinerie, "The brainweb: Phase synchronization and large-scale integration," *Nat. Rev. Neurosci.* **2**, 229–239 (2001).
- <sup>2</sup>G. Buzsáki, *Rhythms of the Brain* (Oxford University Press, 2009).
- <sup>3</sup>P. Fries, "Rhythms for cognition: Communication through coherence," *Neuron* **88**, 220–235 (2015).
- <sup>4</sup>F. Bartolomei, P. Chauvel, and F. Wendling, "Epileptogenicity of brain structures in human temporal lobe epilepsy: A quantified study from intracerebral EEG," *Brain* **131**, 1818–1830 (2008).
- <sup>5</sup>A. K. Kreiter and W. Singer, "Stimulus-dependent synchronization of neuronal responses in the visual cortex of the awake macaque monkey," *J. Neurosci.* **76**, 2381–2396 (1996).
- <sup>6</sup>J. S. Damoiseaux, S. A. Rombouts, F. Barkhof, P. Scheltens, C. J. Stam, S. M. Smith, and C. F. Beckmann, "Consistent resting-state networks across healthy subjects," *Proc. Natl. Acad. Sci. U. S. A.* **103**, 13848–13853 (2006).
- <sup>7</sup>D. Mantini, M. G. Perrucci, C. Del Gratta, G. L. Romani, and M. Corbetta, "Electrophysiological signatures of resting state networks in the human brain," *Proc. Natl. Acad. Sci. U. S. A.* **104**, 13170–13175 (2007).
- <sup>8</sup>S. Baker, J. Kilner, E. Pinches, and R. Lemon, "The role of synchrony and oscillations in the motor output," *Exp. Brain Res.* **128**, 109–117 (1999).
- <sup>9</sup>A. Palmigiano, T. Geisel, F. Wolf, and D. Battaglia, "Flexible information routing by transient synchrony," *Nat. Neurosci.* **20**, 1014–1022 (2017).
- <sup>10</sup>Y. Nir, L. Fisch, R. Mukamel, H. Gelbard-Sagiv, A. Arieli, I. Fried, and R. Malach, "Coupling between neuronal firing rate, gamma LFP, and BOLD fMRI is related to interneuronal correlations," *Curr. Biol.* **17**, 1275–1285 (2007).
- <sup>11</sup>G. Deco, V. K. Jirsa, and A. R. McIntosh, "Emerging concepts for the dynamical organization of resting-state activity in the brain," *Nat. Rev. Neurosci.* **12**, 43–56 (2011).
- <sup>12</sup>S. Heitmann and M. Breakspear, "Putting the 'dynamic' back into dynamic functional connectivity," *Netw. Neurosci.* **2**, 150 (2018).
- <sup>13</sup>P. Sanz-Leon, S. A. Knock, A. Spiegler, and V. K. Jirsa, "Mathematical framework for large-scale brain network modeling in the virtual brain," *NeuroImage* **111**, 385–430 (2015).
- <sup>14</sup>V. Sip, M. Hashemi, T. Dickscheid, K. Amunts, S. Petkoski, and V. Jirsa, "Characterization of regional differences in resting-state fMRI with a data-driven network model of brain dynamics," *Sci. Adv.* **9**, eabq7547 (2023).
- <sup>15</sup>P. Hagmann, L. Cammoun, X. Gigandet, R. Meuli, C. J. Honey, J. Van Wvedeen, and O. Sporns, "Mapping the structural core of human cerebral cortex," *PLoS Biol.* **6**, 1479–1493 (2008).
- <sup>16</sup>J.-D. Lemaréchal, M. Jedynak, L. Trebaul, A. Boyer, F. Tadel, M. Bhattarjee, P. Deman, V. Tuyisenge, L. Ayoubian, E. Hugues *et al.*, "A brain atlas of axonal and synaptic delays based on modelling of cortico-cortical evoked potentials," *Brain J. Neurol.* **145**, 1653 (2021).
- <sup>17</sup>S. Petkoski and V. K. Jirsa, "Transmission time delays organize the brain network synchronization," *Philos. Trans. R. Soc. A Math. Phys. Eng. Sci.* **377**, 20180132 (2019).
- <sup>18</sup>A. Ghosh, Y. Rho, A. R. McIntosh, R. Kötter, and V. K. Jirsa, "Noise during rest enables the exploration of the brain's dynamic repertoire," *PLoS Comput. Biol.* **4**, e1000196 (2008).
- <sup>19</sup>S. Petkoski and V. K. Jirsa, "Normalizing the brain connectome for communication through synchronization," *Netw. Neurosci.* **6**, 722–744 (2022).
- <sup>20</sup>M. Hashemi, A. Ziaemehr, M. M. Woodman, J. Fousek, S. Petkoski, and V. K. Jirsa, "Simulation-based inference on virtual brain models of disorders," *Mach. Learn.: Sci. Technol.* **5**(3), 035019 (2024).
- <sup>21</sup>L. W. Sheppard, A. C. Hale, S. Petkoski, P. V. E. McClintock, and A. Stefanovska, "Characterizing an ensemble of interacting oscillators: The mean-field variability index," *Phys. Rev. E* **87**, 1–11 (2013).

- <sup>22</sup>S. Petkoski, A. Spiegler, T. Proix, P. Aram, J.-J. J. Temprado, and V. K. Jirsa, "Heterogeneity of time delays determines synchronization of coupled oscillators," *Phys. Rev. E* **94**, 1–7 (2016).
- <sup>23</sup>S. Petkoski, J. M. Palva, and V. K. Jirsa, "Phase-lags in large scale brain synchronization: Methodological considerations and in-silico analysis," *PLoS Comput. Biol.* **14**, 1–30 (2018).
- <sup>24</sup>V. K. Jirsa, "Neural field dynamics with local and global connectivity and time delay," *Philos. Trans. R. Soc. A Math. Phys. Eng. Sci.* **367**, 1131–1143 (2009).
- <sup>25</sup>V. K. Jirsa, K. J. Jantzen, A. Fuchs, and J. A. Kelso, "Spatiotemporal forward solution of the EEG and MEG using network modeling," *IEEE Trans. Med. Imaging* **21**, 493–504 (2002).
- <sup>26</sup>V. K. Jirsa and J. A. S. Kelso, "Spatiotemporal pattern formation in neural systems with heterogeneous connection topologies," *Phys. Rev. E* **62**, 8462–8465 (2000).
- <sup>27</sup>V. K. Jirsa, "Connectivity and dynamics of neural information processing," *Neuroinformatics* **2**, 183–204 (2004).
- <sup>28</sup>R. A. Stefanescu and V. K. Jirsa, "A low dimensional description of globally coupled heterogeneous neural networks of excitatory and inhibitory neurons," *PLoS Comput. Biol.* **4**, e1000219 (2008).
- <sup>29</sup>T. Proix, V. K. Jirsa, F. Bartolomei, M. Guye, and W. Truccolo, "Predicting the spatiotemporal diversity of seizure propagation and termination in human focal epilepsy," *Nat. Commun.* **9**, 1088 (2018).
- <sup>30</sup>A. Spiegler, J. K. Abadchi, M. Mohajerani, and V. K. Jirsa, "In silico exploration of mouse brain dynamics by focal stimulation reflects the organization of functional networks and sensory processing," *Netw. Neurosci.* **4**, 807–851 (2020).
- <sup>31</sup>B. J. Cook, A. D. H. Peterson, W. Woldman, and J. R. Terry, "Neural field models: A mathematical overview and unifying framework," *Math. Neurosci. Appl.* **2**, 7284 (2022).
- <sup>32</sup>V. K. Jirsa and R. A. Stefanescu, "Neural population modes capture biologically realistic large scale network dynamics," *Bull. Math. Biol.* **73**, 325–343 (2011).
- <sup>33</sup>K. M. Kutchko and F. Fröhlich, "Emergence of metastable state dynamics in interconnected cortical networks with propagation delays," *PLoS Comput. Biol.* **9**, e1003304 (2013).
- <sup>34</sup>Y. G. Zheng and Z. H. Wang, "Network-scale effect on synchronizability of fully coupled network with connection delay," *Chaos* **26**, 043103 (2016).
- <sup>35</sup>C. M. Kim, U. Egert, and A. Kumar, "Dynamics of multiple interacting excitatory and inhibitory populations with delays," *Phys. Rev. E* **102**, 022308 (2020).
- <sup>36</sup>H. Markram, M. Toledo-Rodriguez, Y. Wang, A. Gupta, G. Silberberg, and C. Wu, "Interneurons of the neocortical inhibitory system," *Nat. Rev. Neurosci.* **5**, 793–807 (2004).
- <sup>37</sup>J. Ren, Y. Aika, C. Heizmann, and T. Kosaka, "Quantitative analysis of neurons and glial cells in the rat somatosensory cortex, with special reference to GABAergic neurons and parvalbumin-containing neurons," *Exp. Brain Res.* **92**, 1–14 (1992).
- <sup>38</sup>R. Brette and W. Gerstner, "Adaptive exponential integrate-and-fire model as an effective description of neuronal activity," *J. Neurophysiol.* **94**, 3637–3642 (2005).
- <sup>39</sup>J. Touboul, "Bifurcation analysis of a general class of nonlinear integrate-and-fire neurons," *SIAM J. Appl. Math.* **68**, 1045–1079 (2008).
- <sup>40</sup>R. Naud, N. Marcille, C. Clopath, and W. Gerstner, "Firing patterns in the adaptive exponential integrate-and-fire model," *Biol. Cybern.* **99**, 335 (2008).
- <sup>41</sup>J. Ladenbauer, M. Augustin, L. Shiau, and K. Obermayer, "Impact of adaptation currents on synchronization of coupled exponential integrate-and-fire neurons," *PLoS Comput. Biol.* **8**, e1002478 (2012).
- <sup>42</sup>E. Izhikevich, "Which model to use for cortical spiking neurons?," *IEEE Trans. Neural Netw.* **15**, 1063–1070 (2004).
- <sup>43</sup>T. Gorski, D. Depannemaecker, and A. Destexhe, "Conductance-based adaptive exponential integrate-and-fire model," *Neural Comput.* **33**, 41–66 (2021).
- <sup>44</sup>R. Kobayashi, Y. Tsubo, and S. Shinomoto, "Made-to-order spiking neuron model equipped with a multi-timescale adaptive threshold," *Front. Comput. Neurosci.* **3**, 9 (2009).
- <sup>45</sup>N. Brunel, V. Hakim, and M. J. E. Richardson, "Firing-rate resonance in a generalized integrate-and-fire neuron with subthreshold resonance," *Phys. Rev. E* **67**, 051916 (2003).
- <sup>46</sup>A. L. Hodgkin and A. F. Huxley, "A quantitative description of membrane current and its application to conduction and excitation in nerve," *J. Physiol.* **117**, 500–544 (1952).
- <sup>47</sup>L. Lapique, "Recherches quantitatives sur l'excitation électrique des nerfs," *J. Physiol.* **9**, 620–635 (1907).
- <sup>48</sup>H. C. Tuckwell, "Introduction to theoretical neurobiology: Volume 2: Non-linear and stochastic theories," in *Cambridge Studies in Mathematical Biology* (Cambridge University Press, 1988), Vol. 2.
- <sup>49</sup>R. FitzHugh, "Mathematical models of threshold phenomena in the nerve membrane," *Bull. Math. Biophys.* **17**, 257–278 (1955).
- <sup>50</sup>J. Nagumo, S. Arimoto, and S. Yoshizawa, "An active pulse transmission line simulating nerve axon," *Proc. IRE* **50**, 2061–2070 (1962).
- <sup>51</sup>N. Voges and L. U. Perrinet, "Complex dynamics in recurrent cortical networks based on spatially realistic connectivities," *Front. Comput. Neurosci.* **6**, 41 (2012).
- <sup>52</sup>N. Brunel, "Dynamics of sparsely connected networks of excitatory and inhibitory spiking neurons," *J. Comput. Neurosci.* **8**, 183–208 (2000).
- <sup>53</sup>Y. Kuramoto, "Method of phase description I," in *Chemical Oscillations, Waves, and Turbulence*, Springer Series in Synergetics (Springer, Berlin, 1984), pp. 22–34.
- <sup>54</sup>F. S. Borges, P. R. Protachevicz, E. L. Lameu, R. C. Bonetti, K. C. Iarosz, I. L. Caldas, M. S. Baptista, and A. M. Batista, "Synchronised firing patterns in a random network of adaptive exponential integrate-and-fire neuron model," *Neural Netw.* **90**, 1–7 (2017).
- <sup>55</sup>J. P. Lachaux, E. Rodriguez, J. Martinerie, and F. J. Varela, "Measuring phase synchrony in brain signals," *Hum. Brain Mapp.* **8**, 194–208 (1999).
- <sup>56</sup>M. K. S. Yeung and S. H. Strogatz, "Time delay in the Kuramoto model of coupled oscillators," *Phys. Rev. Lett.* **82**, 648–651 (1999).
- <sup>57</sup>E. Niebur, H. G. Schuster, and D. M. Kammen, "Collective frequencies and metastability in networks of limit-cycle oscillators with time delay," *Phys. Rev. Lett.* **67**, 2753–2756 (1991).
- <sup>58</sup>M. Y. Choi, H. J. Kim, D. Kim, and H. Hong, "Synchronization in a system of globally coupled oscillators with time delay," *Phys. Rev. E* **61**(1), 371–381 (2000).
- <sup>59</sup>N. Mosheiff, B. Ermentrout, and C. Huang, "Chaotic dynamics in spatially distributed neuronal networks generate population-wide shared variability," *PLoS Comput. Biol.* **19**, e1010843 (2023).
- <sup>60</sup>S. Petkoski, A. Spiegler, T. Proix, P. Aram, J.-J. Temprado, and V. K. Jirsa, "Heterogeneity of time delays determines synchronization of coupled oscillators," *Phys. Rev. E* **94**, 012209 (2016).
- <sup>61</sup>J. Senk, K. Korvasová, J. Schuecker, E. Hagen, T. Tetzlaff, M. Diesmann, and M. Helias, "Conditions for wave trains in spiking neural networks," *Phys. Rev. Res.* **2**, 023174 (2020).
- <sup>62</sup>B. Haider, A. Duque, A. R. Hasenstaub, and D. A. McCormick, "Neocortical network activity in vivo is generated through a dynamic balance of excitation and inhibition," *J. Neurosci.* **26**, 4535–4545 (2006).
- <sup>63</sup>N. Dehghani, A. Peyrache, B. Telenczuk, M. Le Van Quyen, E. Halgren, S. S. Cash, N. G. Hatsopoulos, and A. Destexhe, "Dynamic balance of excitation and inhibition in human and monkey neocortex," *Sci. Rep.* **6**, 23176 (2016).
- <sup>64</sup>S. J. V. Albada, M. Helias, and M. Diesmann, "Scalability of asynchronous networks is limited by one-to-one mapping between effective connectivity and correlations," *PLoS Comput. Biol.* **11**, e1004490 (2015).
- <sup>65</sup>A. Pikovsky, M. Rosenblum, and J. Kurths, *Synchronization: A Universal Concept in Nonlinear Sciences* (Cambridge University Press, 2001).
- <sup>66</sup>Z. W. Davis, G. B. Benigno, C. Fletterman, T. Desbordes, C. Steward, T. J. Sejnowski, J. H. Reynolds, and L. Muller, "Spontaneous traveling waves naturally emerge from horizontal fiber time delays and travel through locally asynchronous-irregular states," *Nat. Commun.* **12**, 6057 (2021).
- <sup>67</sup>D. Roy, A. Ghosh, and V. K. Jirsa, "Phase description of spiking neuron networks with global electric and synaptic coupling," *Phys. Rev. E* **83**, 051909 (2011).
- <sup>68</sup>C. Bick, E. Gross, H. A. Harrington, and M. T. Schaub, "What are higher-order networks?" *SIAM Rev.* **65**, 686–731 (2023).
- <sup>69</sup>T. Stankovski, S. Petkoski, A. F. Smith, P. V. E. McClintock, A. Stefanovska, J. Raeder, A. F. Smith, P. V. E. McClintock, and A. Stefanovska, "Alterations in the coupling functions between cortical and cardio-respiratory oscillations due to anaesthesia with propofol and sevoflurane," *Philos. Trans. R. Soc. A* **374**, 20150186 (2016).

<sup>70</sup>D. Lukarski, S. Petkoski, P. Ji, and T. Stankovski, “Delta-alpha cross-frequency coupling for different brain regions,” *Chaos* **33**, 103126 (2023).

<sup>71</sup>P. Yger, S. El Boustani, A. Destexhe, and Y. Frégnac, “Topologically invariant macroscopic statistics in balanced networks of conductance-based integrate-and-fire neurons,” *J. Comput. Neurosci.* **31**, 229–245 (2011).

<sup>72</sup>Y. Zerlaut, S. Chemla, F. Chavane, and A. Destexhe, “Modeling mesoscopic cortical dynamics using a mean-field model of conductance-based networks of

adaptive exponential integrate-and-fire neurons,” *J. Comput. Neurosci.* **44**, 45–61 (2018).

<sup>73</sup>M. Augustin, J. Ladenbauer, and K. Obermayer, “How adaptation shapes spike rate oscillations in recurrent neuronal networks,” *Front. Comput. Neurosci.* **7**, 9 (2013).

<sup>74</sup>E. Nordlie, M.-O. Gewaltig, and H. E. Plesser, “Towards reproducible descriptions of neuronal network models,” *PLoS Comput. Biol.* **5**, e1000456 (2009).